Title

Closure to “performance of a transparent Flexible Shear Beam container for geotechnical centrifuge modelling of dynamic problems” by Ghayoomi M., Dashti S., and McCartney J.S.

Authors

Ghayoomi, M
Dashti, S
McCartney, JS

Publication Date

2014-12-01

DOI

10.1016/j.soildyn.2014.02.002

Peer reviewed

Closure to "Performance of a Transparent Flexible Shear Beam Container for Geotechnical Centrifuge Modelling of Dynamic Problems" by Ghayoomi M., Dashti S., and McCartney J.S.

Majid Ghayoomi, University of New Hampshire, USA
Shideh Dashti and John S. McCartney, University of Colorado Boulder, USA

The authors thank Professors Haigh and Madabushi [1] for their interest and constructive feedback on the paper related to the performance of a recently developed transparent Flexible Shear Beam (FSB)-type container used for dynamic centrifuge modelling [2]. This container permits evaluation of the seismic response of soil under softened conditions, easier saturation of soil profiles than laminar containers, and implementation of systems for control of infiltration and drainage processes in partially saturated soil layers. Further, this new container permits the use of Particle Image Velocimetry [3] and other types of digital image analysis to study the dynamic response of soil layers and buried structures while reducing boundary effects. However, there are certain trade-offs that must be considered in its use. Our closure addresses the three concerns raised by the discussers, namely, (1) the lateral stiffness of the container and the associated effects of lateral static deflections on the behaviour of the soil specimen; (2) the effects of higher modes of vibration on the simulation of 1-D horizontal shaking in soil; and (3) the free-field soil response under 1-D shaking as predicted by equivalent-linear site response analyses and as measured by the container.

Lateral Stiffness of Container Walls

The outside dimensions of the container were limited by the size of the shaker platform and its payload capacity. The centrifuge shake table performance in terms of the amplitude and frequency content of the achieved motions is directly related to the payload mass [4]. The thickness of acrylic frames of 38.1 mm was selected to balance the need to maximize the inside dimensions of the container (in order to minimize boundary effects) and minimize total container mass, while maintaining an

acceptable lateral stiffness. The inside dimensions of the container were selected to be consistent with previous containers used by Dewoolkar et al. [5] and Ghayoomi et al. [6] in dynamic centrifuge experiments at the same facility. Although the selected frame thickness balances the geometric restraints and payload mass limitations, there is potential for larger lateral deflections compared to those in previous containers built with thicker acrylic side walls. A lower lateral stiffness leads to greater lateral deflections during spin-up of a soil specimen, potentially leading to changes in the soil's static stress state. Although the discussers predict that the lateral deflections of the new FSB container may be high enough to cause a reduction in earth pressures, measurements of lateral framed deflections under static conditions do not agree with their predictions. Possible reasons are discussed in this section.

The static lateral deflections of the container were measured in the middle of the long-span of all container frames when it was filled with medium-dense, dry sand under different centrifuge accelerations. The lateral deflection of the top container frame during spin up and the maximum lateral deflection profile of all container frames at different g-levels are shown in Figures 1a and b. An increase in the maximum lateral deflection of the container from 0.36 to 0.58 mm as it was spun from 30 to 80 g is observed in the data in Figure 1a. The container showed an increase in lateral stiffness as the g-level increased (i.e., a smaller increase in lateral deformations at higher g-levels) even though lateral earth pressures increased under higher centrifuge accelerations. This is proposed to be due to the stress-dependent stiffness of the rubber layers in between frames.

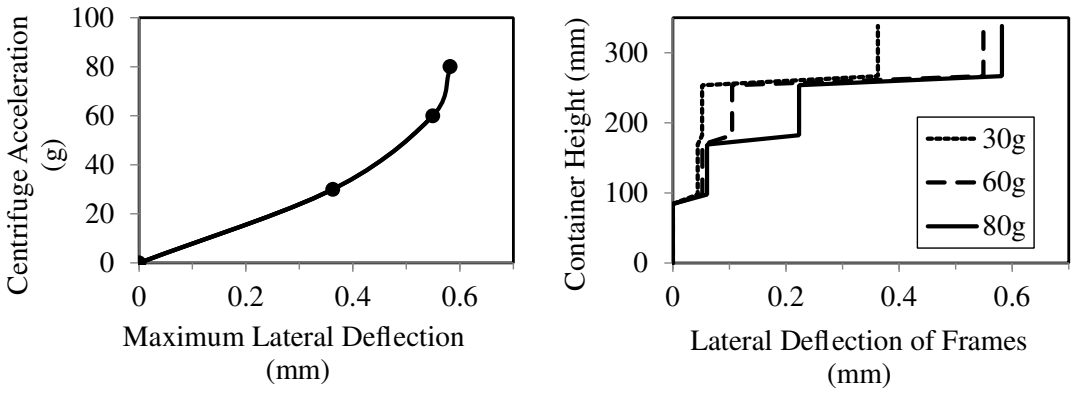

(a) (b)

Figure 1. Model-scale frame deflections during spin-up of a dry, medium-dense sand layer to 80g in the centrifuge: (a) top frame; (b) all frames

The maximum lateral deflection of 0.58 mm (a prototype lateral deflection of 46.4 mm) observed in Figure 1a at 80g corresponds to a maximum deflection to height ratio (δ/H) of 0.0017 for a model-scale soil layer having a height of 338 mm. From the chart provided by Clayton and Milititsky [7] this deflection to height ratio is sufficient to lead to active earth pressure conditions, as it is higher than 0.001. However, the δ/H limit of = 0.001 for active conditions is recommended for dense, cohesionless soils, according to the Canadian Foundation Engineering Manual [8]. The required δ/H ratios to mobilize active pressure for different soil conditions are summarized in Table 1. With the goal of better understanding the limitations of the new FSB container in mind, this container will be most suitable for loose to medium cohesionless soils and all types of cohesive soils when spinning to g-levels as high as 80 to 100g.

Table 1: Magnitude of wall deflection to height ratios required to reach active conditions for different soil types [2].

Soil type and condition	δ/H for active condition
Dense cohesionless	0.001
Loose cohesionless	0.004
Stiff cohesive	0.01
Soft cohesive	0.02

A simple beam or plate assumption is not appropriate to predict the lateral deflection of the container. For example, each frame is supported on both sides (top and bottom) by other frames, which differentiate its behaviour from a simple beam response with fixed ends. Further, the plate theory approach is not appropriate because the lateral earth pressures vary with depth along the container wall, while the same average stress is imposed in the plate theory throughout the height of the plate.

Although a more complex Finite Element (FE) ABAQUS analysis can provide a more accurate response, the input material properties play a critical role in the predicted lateral deflections, which appeared to differ between the authors and the discussers. For example, the predicted lateral deflection of the system is particularly sensitive to the stiffness of the rubber, which is stress-dependent, as well as the Poisson's ratio of the rubber [9]. Additionally, the impact of the aluminum frame on top of the container was not considered in the analysis performed by the discussers.

The sensitivity of the numerical predictions of lateral static deflections by ABAQUS to these input parameters is presented below. Relatively small lateral deflections on the side of the container and negligible soil settlements that were measured during spin-up validate the numerical simulations performed by the authors.

As a starting point, a container model with the aluminium and acrylic material properties listed in Table 1 of the original manuscript was created. A Young's modulus (E_r) of 4 MPa and a Poisson's ratio (υ_r) of 0.49 were used for the rubber in the analysis (Table 1 in the paper). This choice of elastic parameters assumes that the stiffness of the rubber is not stress-dependent. The upper bound of the rubber modulus was picked because the rubber stiffness was expected to significantly change the response. A hydrostatically-distributed lateral earth pressure was applied to the inside of the container throughout the depth in the analysis. The pressure was calculated based on the sand layer with ρ=1565.8 kg/m^3, N=80g and K_0=0.46 ($\phi = 33\,^\circ$). The exaggerated deformed shape of the container is shown in Figure 2. The predicted maximum lateral deflection is approximately 4.4 mm, which is close to that calculated by the discussers.

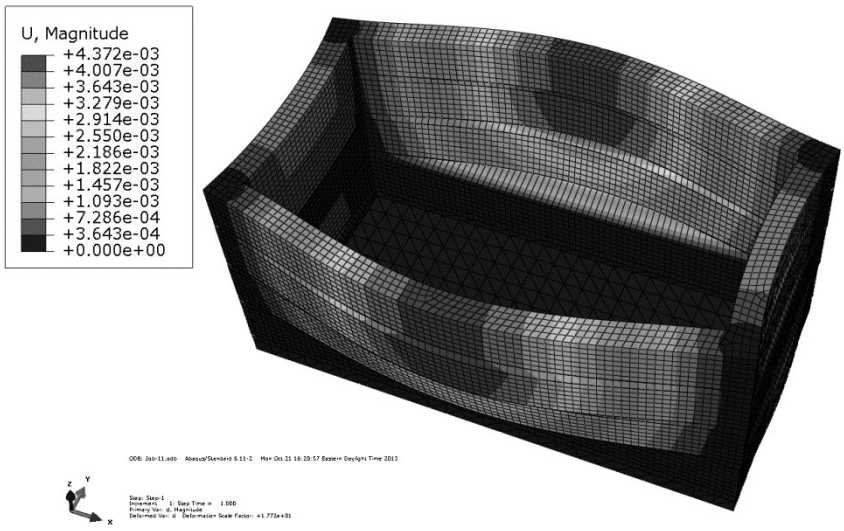

Figure 2. Deformations of FSB container under geostatic conditions at 80 g using the parameters reported in the original manuscript.

The soft neoprene used in this container has a stress-dependent Young's modulus. The response of this rubber under compression was tested during loading and unloading, reported by Ghayoomi et al. [9] and repeated below in Figure 3. The

stress-strain curve clearly indicates that rubber has a highly nonlinear response. The curve shown in Figure 3 is in accordance with other reported stress-strain curves for rubber [10]. The reported modulus of 2-4 MPa in Table 1 of the original manuscript is associated with a normal stress range of 50 to 200 kPa, as mentioned in the footnote of that table. However, considering the weight of the frames at 80 g, the applied normal stress on rubber exceeds this range by a large extent. The normal stress is estimated to vary from about 560 kPa on the top rubber layer to about 2,300 kPa on the bottom layer at 80g. The equivalent linear modulus can be approximately estimated by taking the slope of the stress-strain curve in Figure 3, in which case the modulus increases from 13 to 52 MPa from the top to bottom rubber layers. The modulus associated with pressures outside the range in Figure 3 was approximated using interpolation of the observed trend.

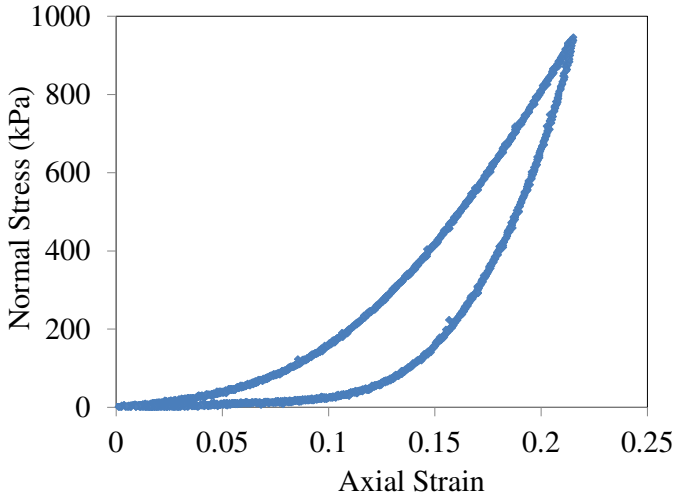

Figure 3. Response of soft Neoprene rubber (30A Durometer) under axial compression [9]

A new analysis was performed in Abaqus with updated stress-dependent Young's modulus of the rubber. The deformed shape of the container is shown in Figure 4. The maximum lateral deflection of the container was approximately 2.3 mm, which is nearly half the value of 4.4 mm observed in Figure 2. This indicates the importance in considering the pressure dependent properties of the rubber.

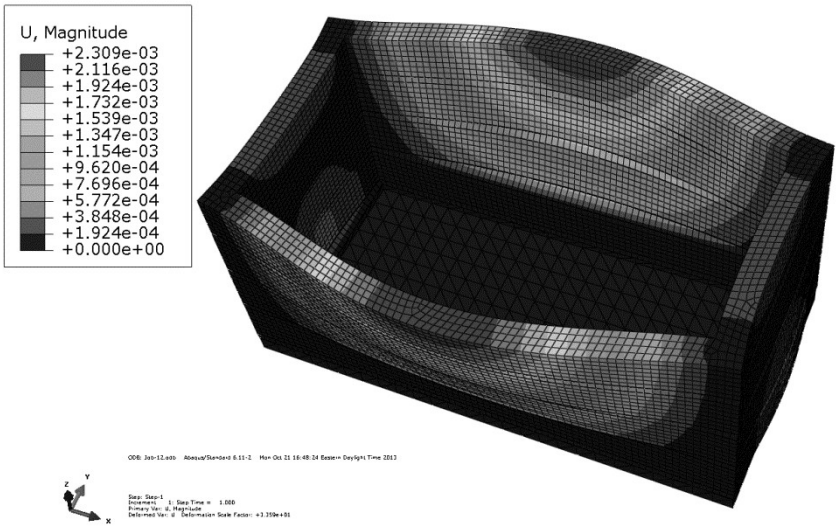

Figure 4. Deformation of FSB container under geostatic conditions at 80g with stress-dependent elastic properties for the rubber layers with $\upsilon_r = 0.49$.

The assumed value of the Poisson's ratio will have an important effect on rubber's behaviour in shear, as the shear modulus is estimated from: $G = \frac{E}{2(1+\vartheta)}$. There is some uncertainty in the actual value of rubber's Poisson's ratio, although it is typically assumed to be close to 0.5 [11] (i.e., rubber is assumed to be an incompressible material). To better understand the effect of Poisson's ratio, a similar analysis with stress-dependent rubber modulus was performed for different υ_r assumptions. The maximum lateral deflection of the top container frame was calculated to range from 2.0 to 1.9 mm for Poisson's ratios ranging from 0.495 to 0.499. Therefore, a small change in the assumed value of Poisson's ratio has a visible influence on lateral displacements.

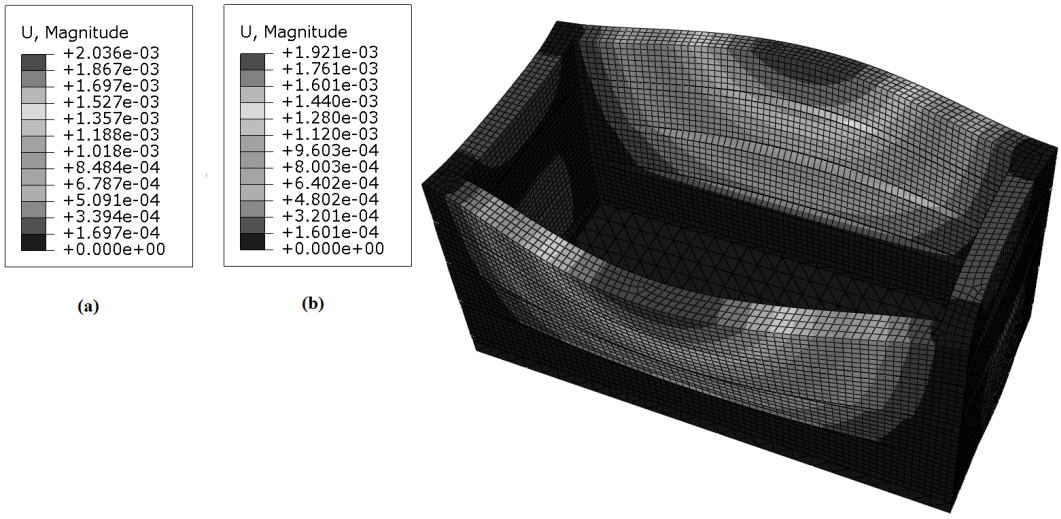

Figure 5. Deformation of the FSB container under geostatic conditions with stress-dependent E_r and (a) $\upsilon_r = 0.495$ and (b) $\upsilon_r = 0.499$.

In addition to the sensitivity of the computed lateral deflections to the elastic properties of the rubber layers, an important component not considered by the discussers is the aluminum frame rigidly bonded to the top acrylic frame. The aluminum frame provided support for the instrumentation rack and simultaneously added to the lateral stiffness of the system (shown in Figure 1b of the original manuscript). In the next analysis, the container was simulated with the top frame included to demonstrate its influence. The Young's modulus of the rubber was also updated because of the slight increase in the vertical stress on each rubber layer due to the additional weight of the top aluminium frame previously not considered. The deformed shape of the container shown in Figure 6 indicates a maximum lateral deflection of approximately 0.85 mm. This value is closer to the measured lateral deflections in Figure 1.

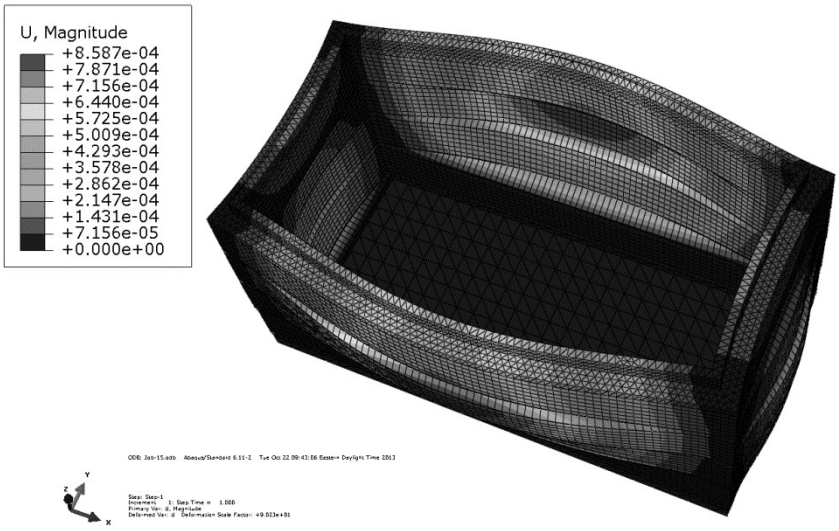

Figure 6. Deformation of the FSB container including the aluminium frame under geostatic conditions with stress-dependent modulus.

As mentioned above, an instrumentation rack is typically used to support the sensors mounted on the soil deposit and structures (e.g. vertical and horizontal LVDTs). Although these racks were not designed to provide lateral stiffness, they restrain the top aluminium frame from expanding laterally. In order to estimate the potential effects of the instrumentation rack, the top aluminum frame was restrained from lateral deformations in the width direction (y-direction). The result of the Abaqus analysis is shown in Figure 7, and a maximum lateral deflection of 0.47 mm was predicted in the second frame from the top of the container.

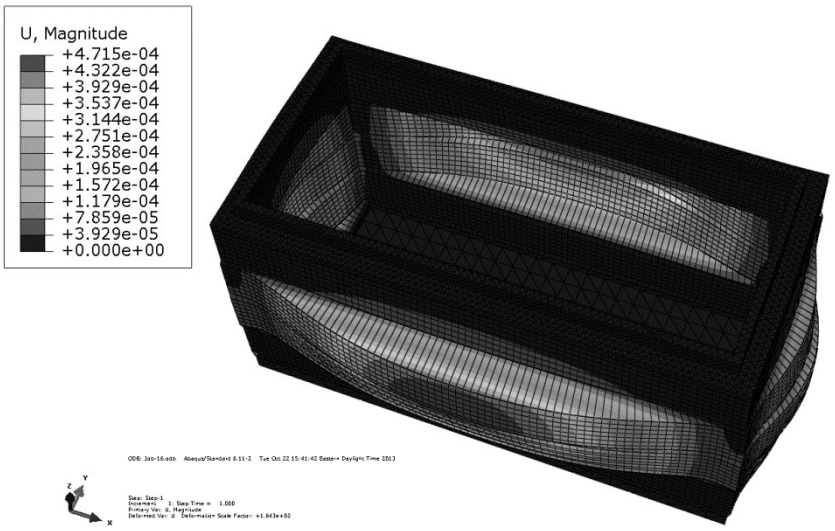

Figure 7. Deformation of the FSB container including the restrained aluminium frame under geostatic conditions with stress-dependent modulus.

The analyses presented above show the importance of carefully considering the material parameters of the rubber layers as well as the effect of the top aluminum plate on the estimated lateral deflections of the container. The maximum calculated deflection (~0.85 mm) is now closer to the maximum measured deflection (~0.58), and is an order of magnitude lower than the value calculated by the discussers. It should be mentioned that the measured 0.58 mm lateral defection was observed without the presence of an instrumentation rack, which will serve to further decrease the actual lateral deflections.

Higher modes of vibration

The higher modes of vibration noted by the discussers in their ABAQUS analysis may have an effect on the assumption that the container is only evaluating the effects of 1D horizontal shaking on the soil and structure. However, the authors believe that

these effects will be small in comparison with the major modes in the shaking direction. The container was analysed: 1) with constant rubber modulus value E_r=4 MPa , υ_r = 0.49, and without the top aluminium frame (similar to the assumptions of the discussers, except for the constant Young's modulus of rubber being 4 MPa instead of 2 MPa); and 2) with stress-dependent rubber modulus, υ_r = 0.49, and the top aluminium frame included. The estimated vibration modes changed considerably in the two sets of analyses, as shown in Table 2. These higher frequency modes are expected to exceed 2 Hz in the prototype scale at 80 g, beyond which the earthquake energy becomes less significant. The estimated mode shapes for the 4th and 5th vibration modes are shown in Figure 8. Their high modal frequencies presented in Table 2 imply that the vibration modes governed by the acrylic ring stiffness will not have a significant adverse effect on 1-D motion simulation. In addition, considering a stress-dependent modulus for the rubber also affects the 1st mode horizontal natural frequency of the container. It is critical to evaluate the performance of the container with regards to lateral stiffness on a project-specific basis, based on the chosen input motion characteristics, the spin acceleration level of interest, and soil properties.

Table 2: Higher mode natural frequencies of the FSB container in the diagonal and lateral extension of the rings.

Container natural frequencies with E_r = 4 MPa, υ_r = 0.49, and neglecting the top aluminium frame (Hz)		Container natural frequencies with stress-dependent E_r , υ_r = 0.499, and including the top aluminium frame (Hz)		Mode
Model Scale	Prototype scale (at 80 g)	Model Scale	Prototype scale (at 80 g)	
61.1	0.76	132.6	1.66	1: Shear mode in shaking direction
70.1	0.88	143.3	1.79	2: Shear mode in transverse direction
74.5	0.93	159.5	1.99	3: Torsional mode
92.3	1.15	188.1	2.35	4: Diagonal extension
97.5	1.21	186.7	2.33	5: Lateral extension

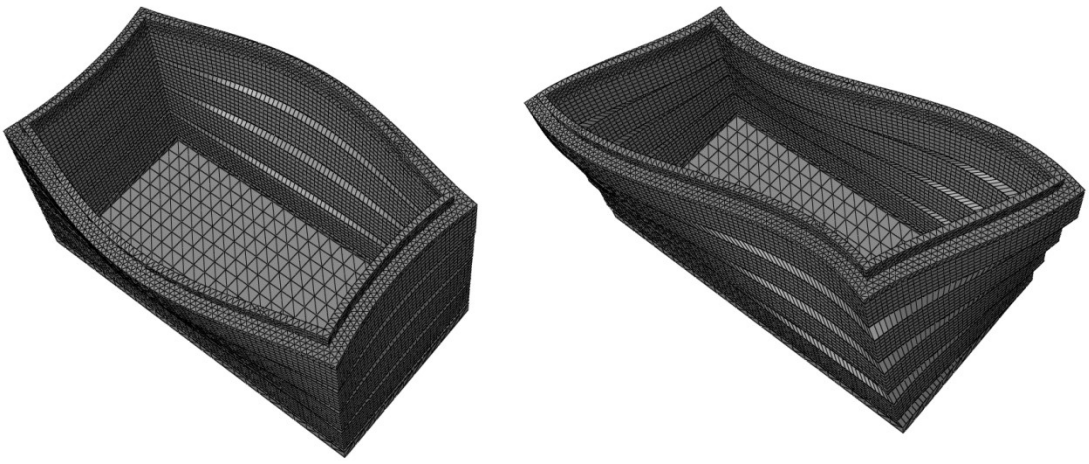

Figure 8. The 4th and 5th vibration modes of the FSB container (Abaqus simulation)

Free-field soil response

Although Equation 6 in the original manuscript is not explicitly provided by Hardin and Richart [12], the expression for G_{max} was converted from an expression for shear wave velocity in that paper. Specifically, Hardin and Richart [12] developed an empirical relationship for the shear wave velocity of round-grained sand at stresses greater than 2000 psf (96 kPa) based on the results of resonant column tests, as follows:

$$c_s = (170 - 78.2\,e)\sqrt[4]{\sigma'_m} \tag{1}$$

where c_s is the shear wave velocity in [ft/s], e is the void ratio, and σ'_m is the mean effective stress (or confining pressure). The small-strain shear modulus, G_{max}, is related to the shear wave velocity as follows:

$$G_{max} = \rho\, c_s^2 \tag{2}$$

where ρ is the total density of the soil. By combining Equations 1 and 2, and by considering $\rho = \frac{G_s}{1+e}\rho_w$ for dry sand with a representative specific gravity (i.e., G_s = 2.65) and water density of 1.94 slugs/ft^3, an expression may be defined for the value of G_{max} for round-grained sand at stresses greater than 2000 psf as follows [13, 14]:

$$G_{max} = \frac{(32.17 - 14.8\,e)^2}{1+e}\sqrt{\sigma'_m} \tag{3}$$

where σ'_m is in psf and G_{max} in psi. This expression is the same as Equation 1 presented in the discussion. The modulus and mean effective stress values from this

equation may be converted to other units. For example, Das [15] and Pak et al. [16] presented this equation in other units, as in Equations 4 and 5, respectively:

$$G_{max}=2630\frac{(2.17-e)^2}{1+e}\sqrt{\sigma'_m} \quad (4)$$

$$G_{max}=700\frac{(2.17-e)^2}{1+e}\sqrt{\sigma'_m} \quad (5)$$

where both σ'_m and G_{max} are in psi or kg/cm^3 in Equations 4 and 5, respectively. Equation 5 above is identical to Equation 6 in the manuscript. Using the G_{max} values predicted in Equation 5 above, the depth-dependent, small-strain, shear modulus of a dry sand layer with a void ratio of 0.69 may be calculated as follows:

$$G_{max}=2.8\times10^7\sqrt{z} \quad (6)$$

where z is the depth in meters and G_{max} is in Pa. This expression is the same as that provided in the discussion and in the original manuscript, confirming that our equation for G_{max} in Equation 5 is accurate.

Using Equation (6) to estimate the small-strain shear modulus of Nevada sand, a 1-D equivalent-linear site response analysis was performed using DEEPSOIL [17], considering all the model preparation details explained in the original manuscript. The computed and measured lateral deformation profiles in the shaking direction are shown in Figure 9, which are the same as those presented in the original manuscript. In addition, the same DEEPSOIL analysis was repeated with a G_{max} profile obtained from Seed and Idriss [18] (Equation 5 in the original paper). The depth-dependent modulus was in the form of $G_{max}=3.6\times10^7\sqrt{z}$, as indicated in the paper. A lower lateral deformation was obtained in the latter case, because of the higher shear modulus values estimated using the Seed and Idriss [18] equation. Both shapes and ranges of deflection are in accordance with the measured container deflections.

The input soil properties are expected to play a significant role in a site response analysis. For example, the selection of an appropriate small-strain shear modulus (G_{max}) profile with depth, the choice of shear modulus reduction curves (G/G_{max} versus shear strain) with depth due to the change in vertical effective stresses, and updating the shear modulus reduction curves to accommodate a constant friction angle and shear strength in the same soil profile [19] may result in the different predicted deformation profiles by the authors and discussers. The details of shear modulus

reduction curves used by the discussers are not known to the authors for proper comparison.

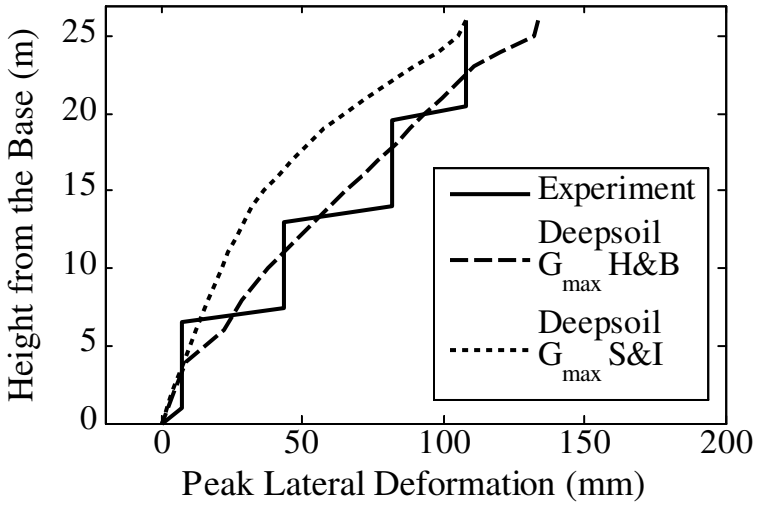

Figure 9. Maximum lateral deformation profiles in test FF-LND77: experimental measurements vs. DEEPSOIL estimations

To better evaluate the performance of the container undergoing a range of input motions, the maximum lateral deformations of the container frames during the application of the Izmit motion (Test FF-IZM60) at a spin acceleration of 60 g is shown in Figure 10. Equation 6 was used to estimate the small-strain shear modulus profile, and other soil model parameters were estimated in a similar manner as in previous analyses. The DEEPSOIL analysis predicted an approximately similar deformation profile to the measured one. In this case, the estimated profile of maximum lateral deformation shows a decrease in change near the top, as indicated by the discussers. This shows the sensitivity of the magnitude and shape of lateral deformations on the container (estimated or measured) to the properties of the base motion and spin-acceleration, as expected.

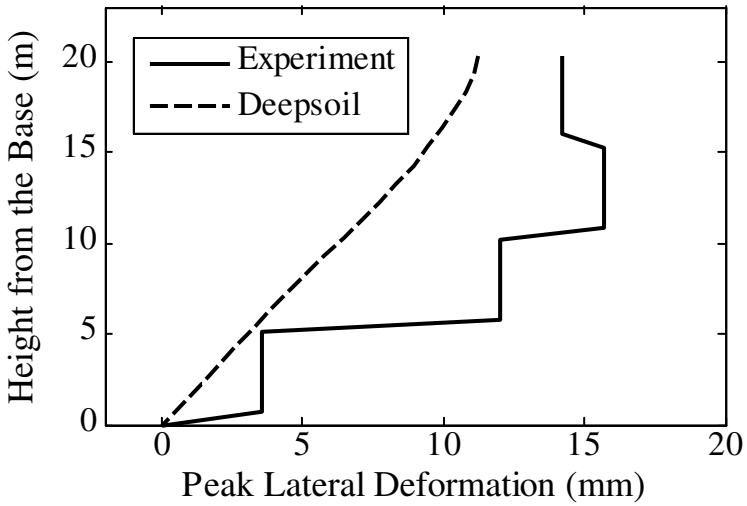

Figure 10. Maximum lateral deformation profiles in Test FF-IZM60: experimental measurements vs. DEEPSOIL estimations

Figure 11 compares the measured lateral deformations of the new FSB container at the University Colorado with those reported for previous ESB or laminar containers. The comparison shows a consistent trend between the measured lateral deformations in Test FF-LND77 [2] of the original manuscript and those reported by previous researchers [20, 21, and 22]. The lateral deformation profile shown by Thevanayagam et al. [22] was obtained at 1g on a large laminar container. Since the test was performed on a saturated soil specimen, a much higher lateral deformation was observed due to lateral spreading. Zeng and Schofield [21] used an Equivalent Shear Beam (ESB) container to model medium dense sand. Because a 10-m thick prototype soil specimen was simulated in their test, a smaller degree of lateral deformation was observed compared to those presented by the authors. Further, an ESB container represents the initial lateral stiffness of a soil column prior to softening, and is therefore expected to undergo smaller lateral deformations under dynamic loading compared to an FSB container. Hushmand et al. [20] tested a 16.5-m thick, loose sand specimen (26% relative density) in a laminar container. Their measured maximum lateral deformation profile follows the trend presented by the authors closely. For proper comparison, the maximum acceleration (PGA) measured at the base of the container in each case is noted in Figure 11.

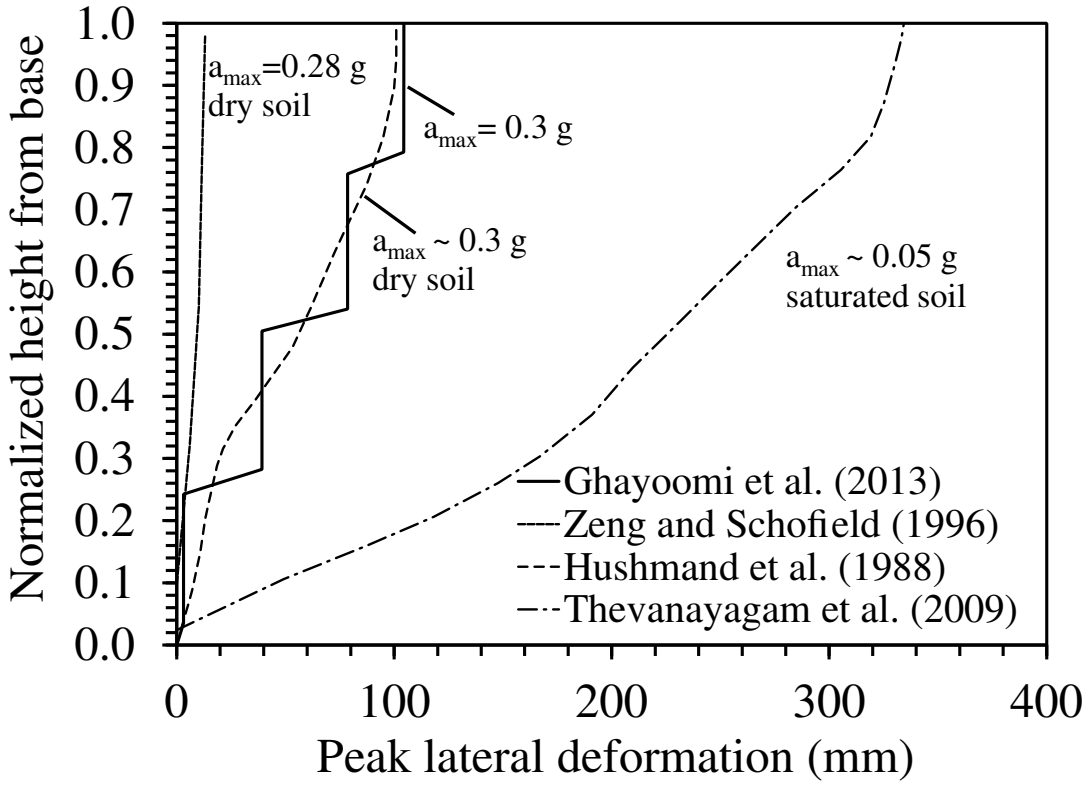

Figure 11. Maximum lateral deflection profiles in various containers used for simulation of earthquake engineering problems.

Concluding Remarks

The discussers have initiated a valuable discussion on important aspects of container characteristics when used in dynamic centrifuge modelling. Despite their concern regarding the magnitude of possible lateral geostatic deflections of the container frames, the experimental measurements made during testing of a free-field medium-dense sand layer at different levels of centrifugal acceleration up to 80g indicates an acceptable performance when modelling loose to medium-dense, cohesionless materials and all types of cohesive soils. Consideration of the role of the upper aluminium frame and the instrumentation rack, as well as the stress-dependent modulus of the rubber layers have likely led to lower predicted lateral geostatic deflections in numerical simulations of the container by the authors compared to the discussers. In addition, the vibration modes associated with frame stiffness are not expected to fall into the high energy frequency range of interest for most earthquake records. The authors believe that the new container mostly achieves its objectives in permitting visualization of buried structures with minimized static and dynamic lateral

deflections that are consistent with those from other containers reported in the literature.

ReferencesX

[1] Haigh, S. and Madabhushi, G., Discussion of "Performance of a transparent flexible shear beam container for geotechnical centrifuge modelling of dynamic problems by Ghayoomi, Dashti & McCartney. Soil Dynamics and Earthquake Engineering, 2013.

[2] Ghayoomi, M., Dashti, S., McCartney, J.S., Performance of a transparent Flexible Shear Beam container for geotechnical centrifuge modeling of dynamic problems. Soil Dynamics and Earthquake Engineering, 2013;53:230–9.

[3] White DJ, Take WA, Bolton MD., Soil deformation measurement using particle image velocimetry (PIV) and photogrammetry. Géotechnique 2003;53(7):619–31.

[4] Ketcham, S.A., Ko, H. Y., Sture, S., An electrohydraulic simulator for centrifuge testing, Centrifuge 88, Rotterdam, 1988.

[5] Dewoolkar, M.M., Ko, H.-Y., and Pak R.Y.S., Seismic behavior of cantilever retaining walls with liquefiable backfills, Journal of Geotechnical and Geoenvironmental Engineering, ASCE, 2001, 127(5): 424-435.

[6] Ghayoomi, M., McCartney, J.S., and Ko, H.-Y., Centrifuge test for seismic compression of partially saturated sands.", ASTM Geotechnical Testing Journal, 2001, 34(4). 1-11.

[7] Clayton CRI, Milititsky J. Earth pressure and earth retaining structures. Surrey University Press, London; 1986.

[8] Canadian Foundation Engineering Manual, 3rd edition, Canadian Geotechnical Society, 1992.

[9] Ghayoomi, M., Dashti, S., and McCartney, J.S., Design and construction of a transparent flexible-shear-beam container for dynamic geotechnical centrifuge testing, Second International Conference on Performance-Based Design in Earthquake Geotechnical Engineering, Taormina, Italy, 2012.

[10] Chaikumpollert, O., Yamamoto, Y., Suchiva, K., and Kawahara, S., Mechanial properties and cross-linking structure of cross-linked rubber, Polymer Journal, 2012, 44, 772-777.

[11] Swallowe, G.M., Mechanical properties and testing of polymers, Kluwer Academic Publishers, 1999.

[12] Hardin, B.O. and Richart, F.E., Elastic wave velocities in granular soils. J Soil Mechanics and Foundations Division, 1963, 89(SM1):33–66.

[13] Hardin, B.O. and Black, W.L., Sand stiffness under various triaxial stresses. J Soil Mechanics and Foundations Division. 1966;92(SM2):27–42.

[14] Hardin, B.O. and Black, W.L., Vibration modulus of normally consolidated clay. J Soil Mechanics and Foundations Division. 1968;94(SM2):353-369.

[15] Das, B.M., Principles of soil dynamics. PWS-KENT Publishing Company, 1992.

[16] Pak, R.Y.S., Ashlock, J.C., Kurahashi, S., and Abedzadeh, F., Parametric G_{max} sounding of granular soils by vibration methods, Géotechnique, 2008, 58(7), 571-580.

[17] Hashash, Y., Deepsoil V5.0, UIUC, Users' Manual, 2012.

[18] Seed H.B. and Idriss I.M., Soil moduli and damping factors for dynamic response analyses, Rep. No. EERC 70-10. Earthquake Engrg. Res. Ctr., Univ. of California, Berkeley, Calif., 1970.

[19] Hashash, Y.M.A., Phillips, C., Groholski, D.R., Recent advances in nonlinear site response analysis, 5th International Conference on Recent Advances in Geotechnical Earthquake Engineering and Soil Dynamics, San Diego, California, May 24-29, 2010, 1-22.

[20] Hushmand, B., Scott, R.F., and Crouse, C.B., Centrifuge liquefaction tests in a laminar box, Géotechnique, 38(2), 253-262.

[21] Zeng, X. and Schofield, A.N., Design and performance of an equivalent-shear-beam container for earthquake centrifuge modelling, Géotechnique, 1996, 46(1), 83-102.

[22] Thevanayagam, S., Kanagalingam, T., Reinhorn, A., Tharmendhira, R., Dobry, R., Pitman, M., Abdoun, T., Elgamal, A., Zeghal, M., Ecemis, N., and El shamy, U., Laminar box system for 1-g physical modeling of liquefaction and lateral spreading, Geotechnical Testing Journal, 32(5), 1-12.